Joule, Volume *6*

Supplemental information

Countdown to perovskite space launch:

Guidelines to performing

relevant radiation-hardness experiments

Ahmad R. Kirmani, Brandon K. Durant, Jonathan Grandidier, Nancy M. Haegel, Michael D. Kelzenberg, Yao M. Lao, Michael D. McGehee, Lyndsey McMillon-Brown, David P. Ostrowski, Timothy J. Peshek, Bibhudutta Rout, Ian R. Sellers, Mark Steger, Don Walker, David M. Wilt, Kaitlyn T. VanSant, and Joseph M. Luther

Supplementary Information
Countdown to perovskite Space launch: *Guidelines to performing relevant radiation-hardness experiments*

Ahmad R. Kirmani[1,], Brandon K. Durant[2], Jonathan Grandidier[3], Nancy Haegel[1], Michael D. Kelzenberg[4], Yao M. Lao[5], Michael D. McGehee[6], Lyndsey McMillon-Brown[7], David P. Ostrowski[1], Timothy J. Peshek[7], Bibhudutta Rout[8], Ian R. Sellers[2], Mark Steger[1], Don Walker[5], David M. Wilt[9], Kaitlyn T. VanSant[1,7], and Joseph M. Luther[1,*]*

[1]National Renewable Energy Laboratory (NREL), CO 80215, USA
[2]Homer L. Dodge Department of Physics and Astronomy, University of Oklahoma, 440 W. Brooks St, Norman, OK, 73019, USA
[3]Jet Propulsion Laboratory, California Institute of Technology, Pasadena, CA 91109, USA
[4]Department of Applied Physics, California Institute of Technology, Pasadena CA, 91125, USA
[5]Electronic and Photonics Laboratory, The Aerospace Corporation, El Segundo, CA 90245, USA
[6]Materials Science and Engineering, University of Colorado, Boulder, CO, 80309, USA
[7]Photovoltaic and Electrochemical Systems Branch, NASA Glenn Research Center, Cleveland, OH 44135, USA
[8]Department of Physics, University of North Texas, Denton, TX 76203, USA
[9]Spacecraft Components Technology Branch (RVSV) US Air Force Research Laboratory, KAFB NM, USA
[*]Corresponding Authors: ahmad.kirmani@nrel.gov, joey.luther@nrel.gov
LEAD CONTACT: Joseph Luther, joey.luther@nrel.gov

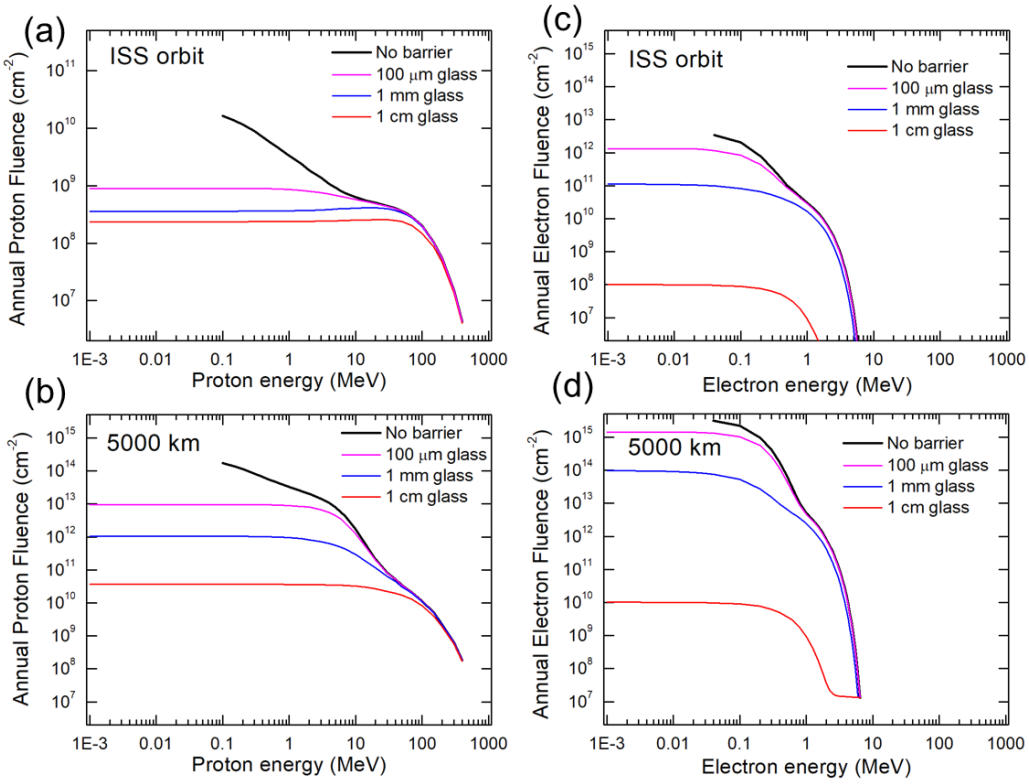

Figure S1. Slowed Proton Fluences for Various Cover Glass Thicknesses. Slowed spectra for proton fluences in (a) ISS orbit, and (b) a 5000 km altitude orbit (60° inclination), and electron fluences in (c) ISS orbit, and (d) a 5000 km altitude orbit (60° inclination). Various cover glass thicknesses are considered. The fluences without any barrier are shown in thick black lines. The original spectra were obtained using SPENVIS, while the slowed spectra with barriers were simulated using www.sr-niel.org

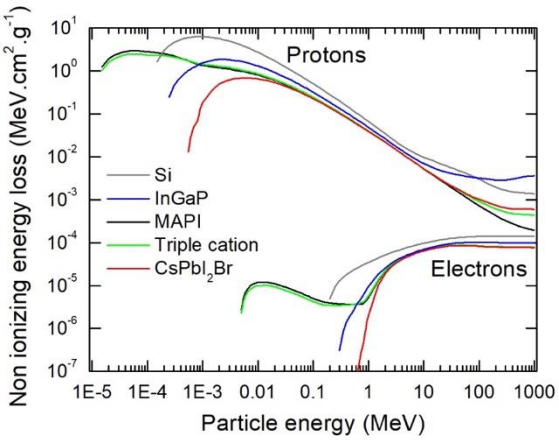

Figure S2. NIELs using SR-NIEL.org. NIELs simulated using www.sr-niel.org showing similarity with Figure 2a which uses SPENVIS.

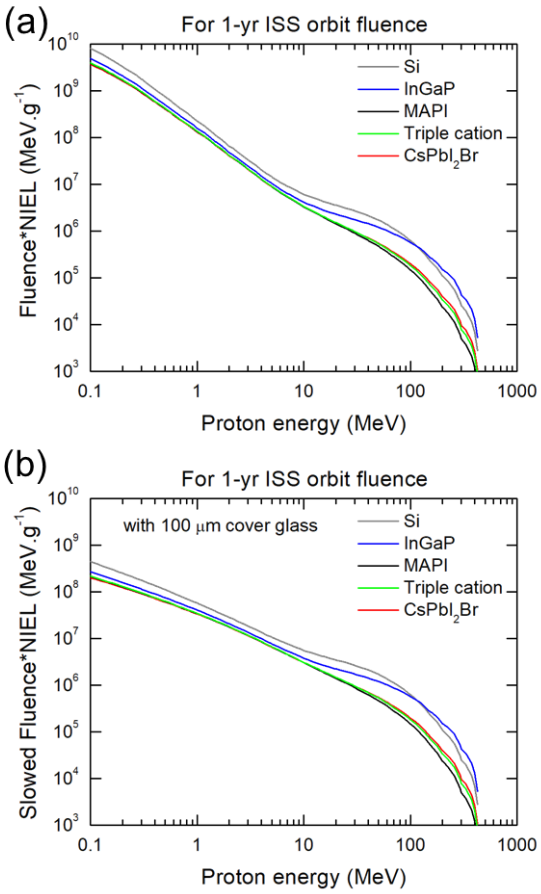

Figure S3. 1-yr ISS Orbit Displacement Damage Dose (DDD) Curves for Protons. DDD curves calculated by multiplying (a) unshielded proton fluences (Figure 1c), and (b) slowed fluences from protons shielded by 100 μm cover glass (Figure S1a), with NIELs (Figure 2c) for the ISS orbit.

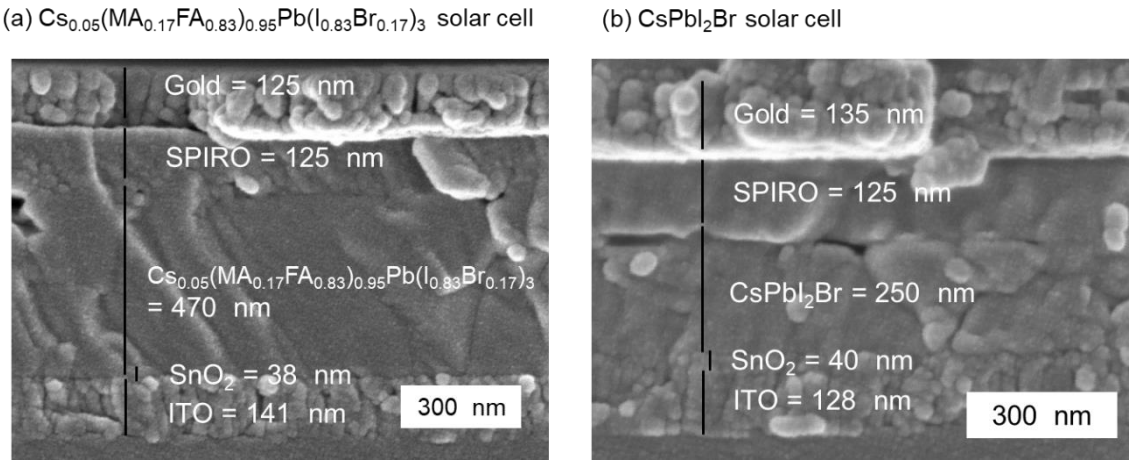

Figure S4. Cross-sectional SEM images. Cross-sectional SEM images of (a) $CsPbI_2Br$, and (b) $Cs_{0.05}(MA_{0.17}FA_{0.83})_{0.95}Pb(I_{0.83}Br_{0.17})_3$ solar cells showing thicknesses of various layers in the device stack. Film thicknesses used in SRIM/TRIM simulations in this paper are based on these experimentally-measured film thicknesses.

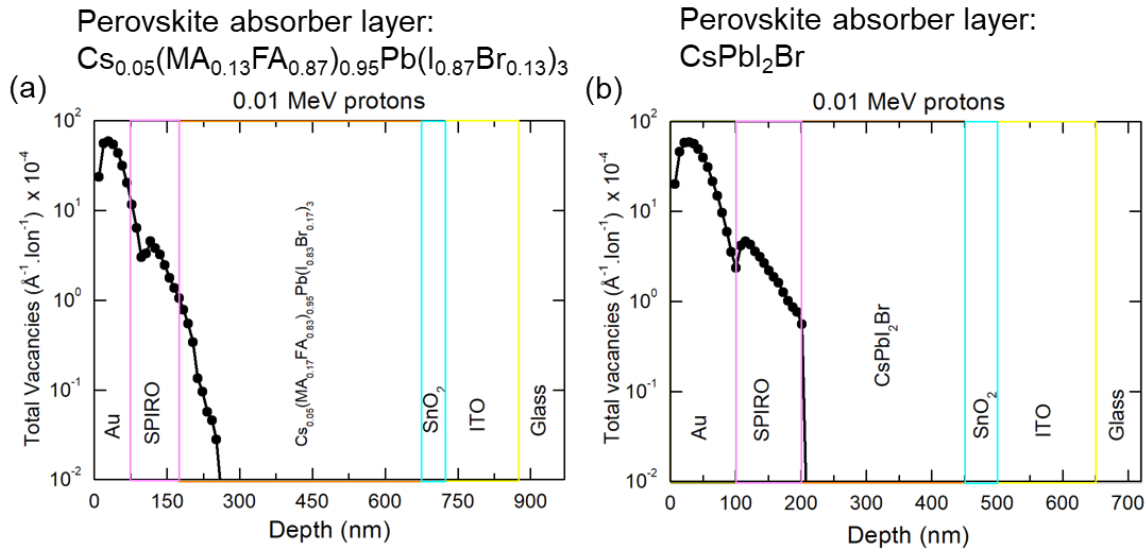

Figure S5. Vacancy Creation from 0.01 MeV Protons. Vacancies created by 0.01 MeV protons in (a) $CsPbI_2Br$ solar cell, (b) $Cs_{0.05}(MA_{0.17}FA_{0.83})_{0.95}Pb(I_{0.83}Br_{0.17})_3$ solar cell. Since these protons fail to reach the perovskite absorber due to their low energy, majority of the vacancies are confined to the metal electrode.

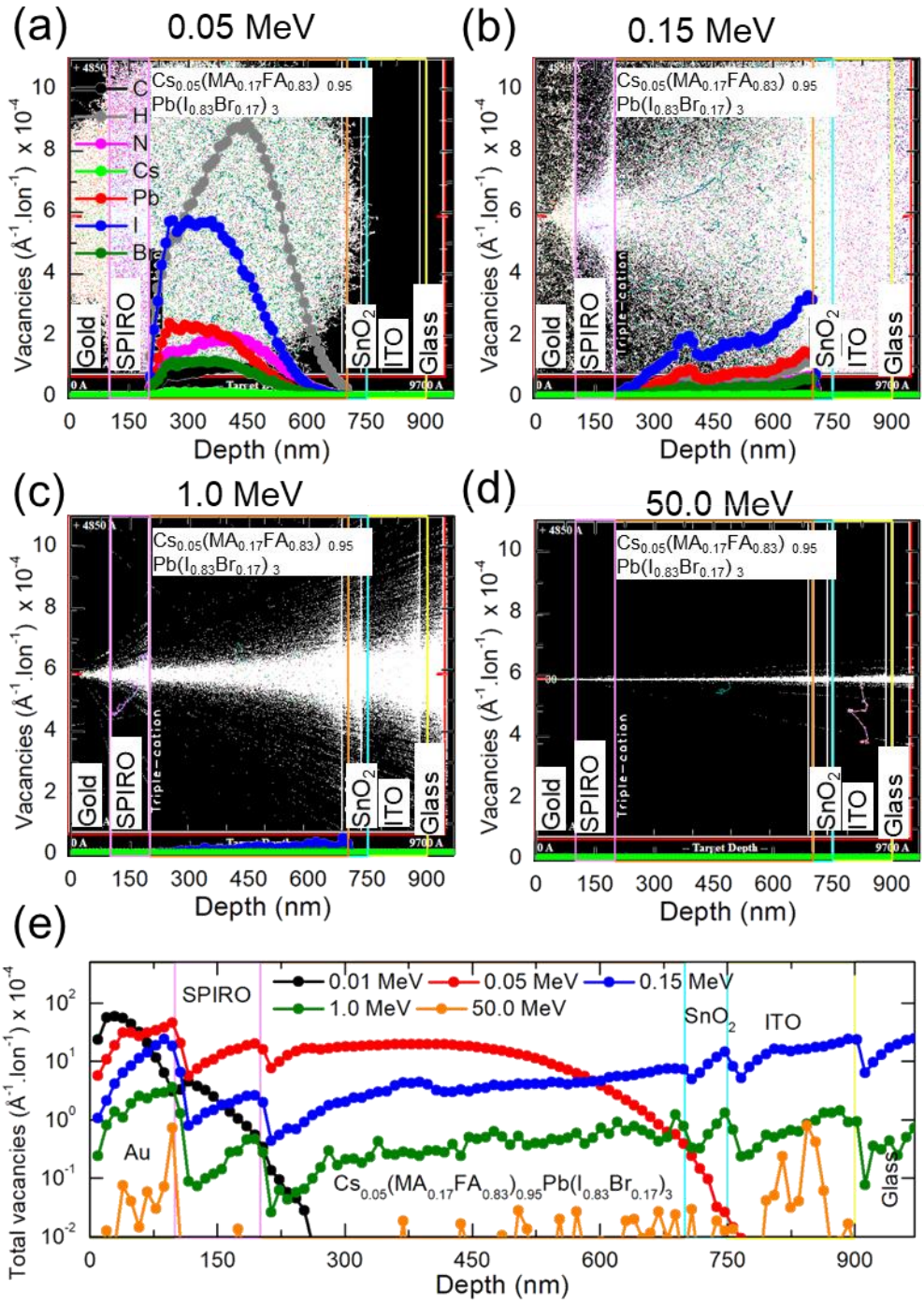

Figure S6. Simulated Proton Interaction with $Cs_{0.05}(MA_{0.17}FA_{0.83})_{0.95}Pb(I_{0.83}Br_{0.17})_3$ Perovskite Devices. a-d). Simulated proton straggling and the resulting vacancies formed due to dislocations of C, H, N, Cs, Pb, I, and Br atoms in $Cs_{0.05}(MA_{0.17}FA_{0.83})_{0.95}Pb(I_{0.83}Br_{0.17})_3$ solar cells. e). Vacancies formed in the full device stack. See Discussion below for details. Device architecture

considered is: Au (100 nm)/SPIRO (100 nm)/$Cs_{0.05}(MA_{0.17}FA_{0.83})_{0.95}Pb(I_{0.83}Br_{0.17})_3$ (500 nm)/SnO_2 (50 nm)/ITO (150 nm)/glass (70 nm).

Discussion:

The case of 0.05 MeV protons highlights the high frequency of collision events for these protons. In fact, these protons are found to stop within the solar cell causing significant displacements. 0.15 MeV protons show a reduced level of interactions, while 1 MeV proton transmit through the solar cells depositing minimal energy in the perovskite. 50 MeV protons are found to leave the solar cells almost unscathed. As expected, 0.05 MeV protons result in the most vacancies, while 50 MeV protons do not appear to create any significant concentration of vacancies in the absorber. Vacancies created in the full device stack are shown as a function of the device thickness/depth in Figure 4e. As can be seen, the 50 MeV protons create ~1000x less vacancies in the perovskite absorber compared to 0.05 MeV protons, in agreement with the NIEL calculated in Figure 2a.

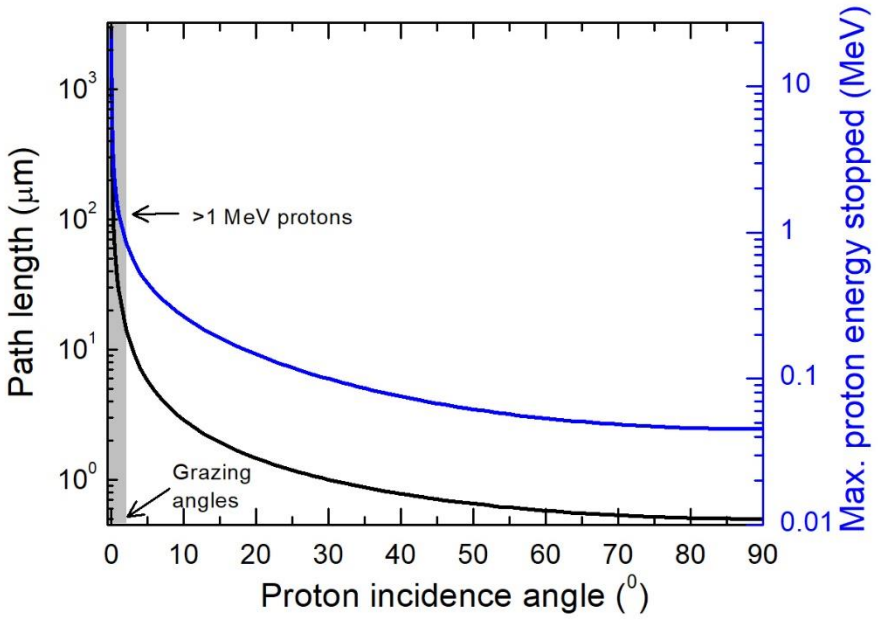

Figure S7. Proton Path Lengths *vs.* Incident Angle. Calculated proton path lengths as a function of incident angle. Right Y-axis shows the proton energies these path lengths (stopping range) correspond to. These are the maximum energies that will completely stop in the device stack at the calculated path lengths. As an example, normal incidence (90°) corresponds to a path length of 0.5 μm, which can stop a proton of ~0.045 MeV. Any higher energy proton will escape the solar cell. As the angles reduce and go toward the grazing-incidence scenario (0°), path lengths increase very slowly. 0.01° corresponds to a ~10,000 μm path length, which is the stopping range for 50 MeV

protons. However, such low incidence angles represent a very small fraction of all the angles possible. Most of the incidence scenarios are similar to the normal incidence case. In other words, for most of the incident angles, >0.05 MeV protons will escape the device and high-energy protons will create little damage.

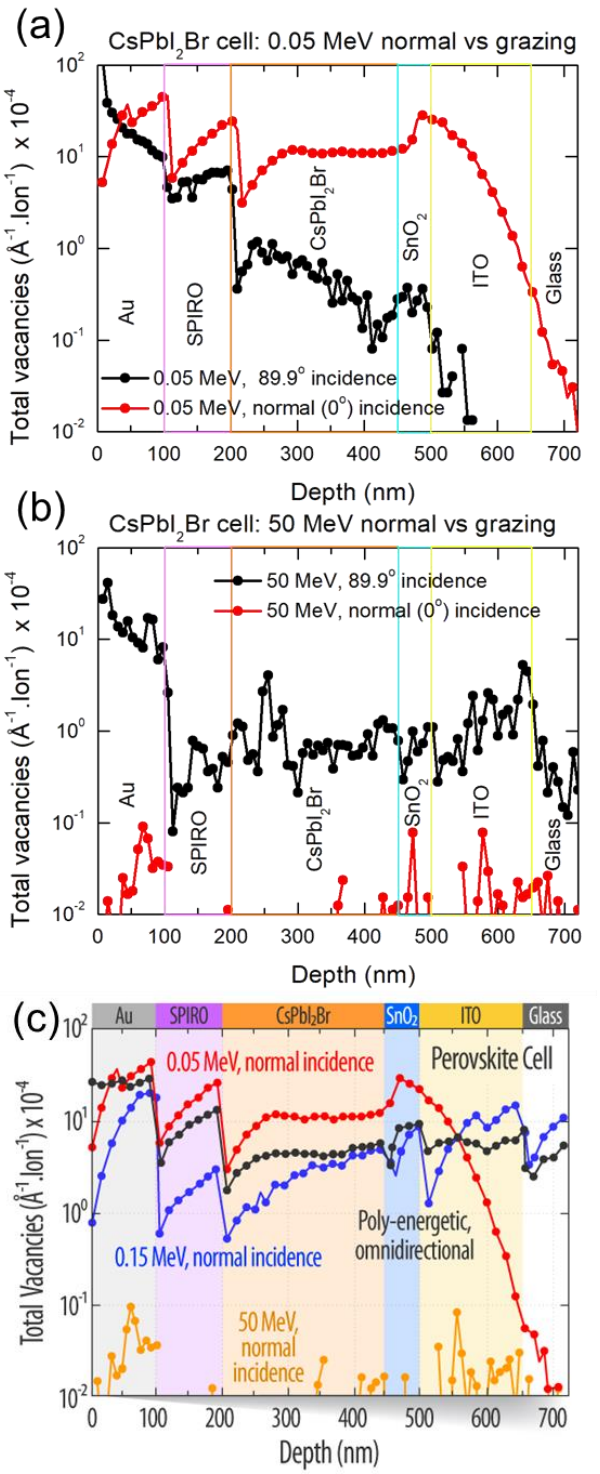

Figure S8. Vacancy Creation for Various Proton Incidence Angles. Damage profiles in a perovskite solar cell upon normal incidence (red) and grazing incidence (black) of (a) 0.05 MeV, and (b) 50 MeV protons, simulated using SRIM. (c) Irradiation of a $CsPbI_2Br$ solar cell with poly-energetic, omnidirectional protons. Normal incidences of 0.05, 0.15, and 50 MeV protons are also shown.

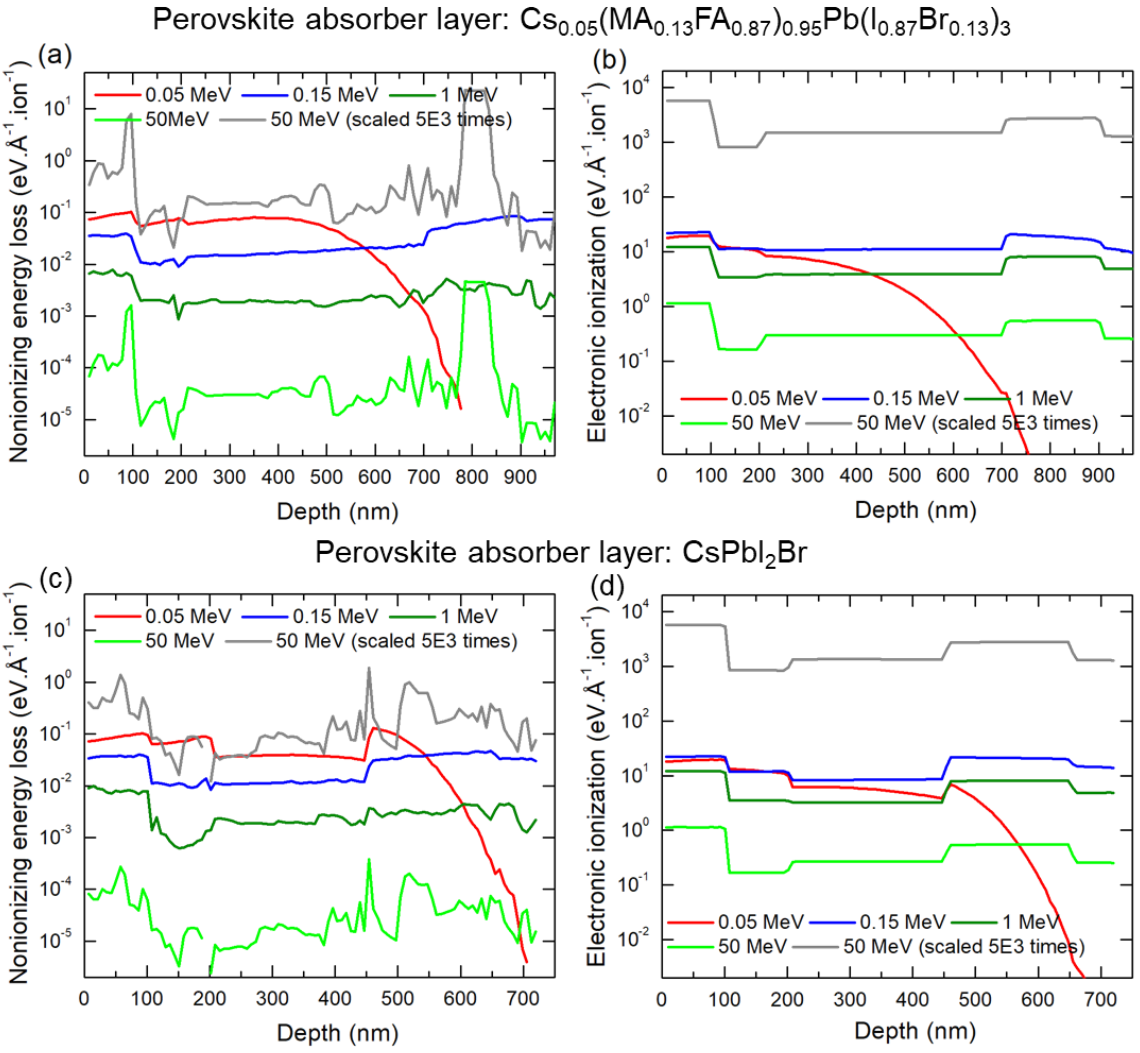

Figure S9. Simulated NIEL vs IEL in Perovskite Devices. SRIM/TRIM simulation results showing a) non-ionizing energy losses, and b) electronic ionization losses for 0.05, 0.15, 1 and 50 MeV protons in a $Cs_{0.05}(MA_{0.17}FA_{0.83})_{0.95}Pb(I_{0.83}Br_{0.17})_3$ solar cell with device architecture: Au (100 nm)/SPIRO (100 nm)/ $Cs_{0.05}(MA_{0.17}FA_{0.83})_{0.95}Pb(I_{0.83}Br_{0.17})_3$ (500 nm)/SnO_2 (50 nm)/ITO (150 nm)/glass (70 nm). Data for a $CsPbI_2Br$ solar cell with a device architecture: Au (100 nm)/SPIRO (100 nm)/ $CsPbI_2Br$ (250 nm)/SnO_2 (50 nm)/ITO (150 nm)/glass (70 nm) are shown in (c) and (d). Both loss mechanisms scale differently with fluence (number of ions). 5E3 protons of 50 MeV (grey spectra) will create a similar number of nuclear displacements as 1 proton of 0.05

MeV (panel a, c), however the corresponding electronic ionization (healing) will be much higher (panel b, d). This implies that fluence at one energy cannot be scaled to match the fluence at another energy in terms of damage induced.

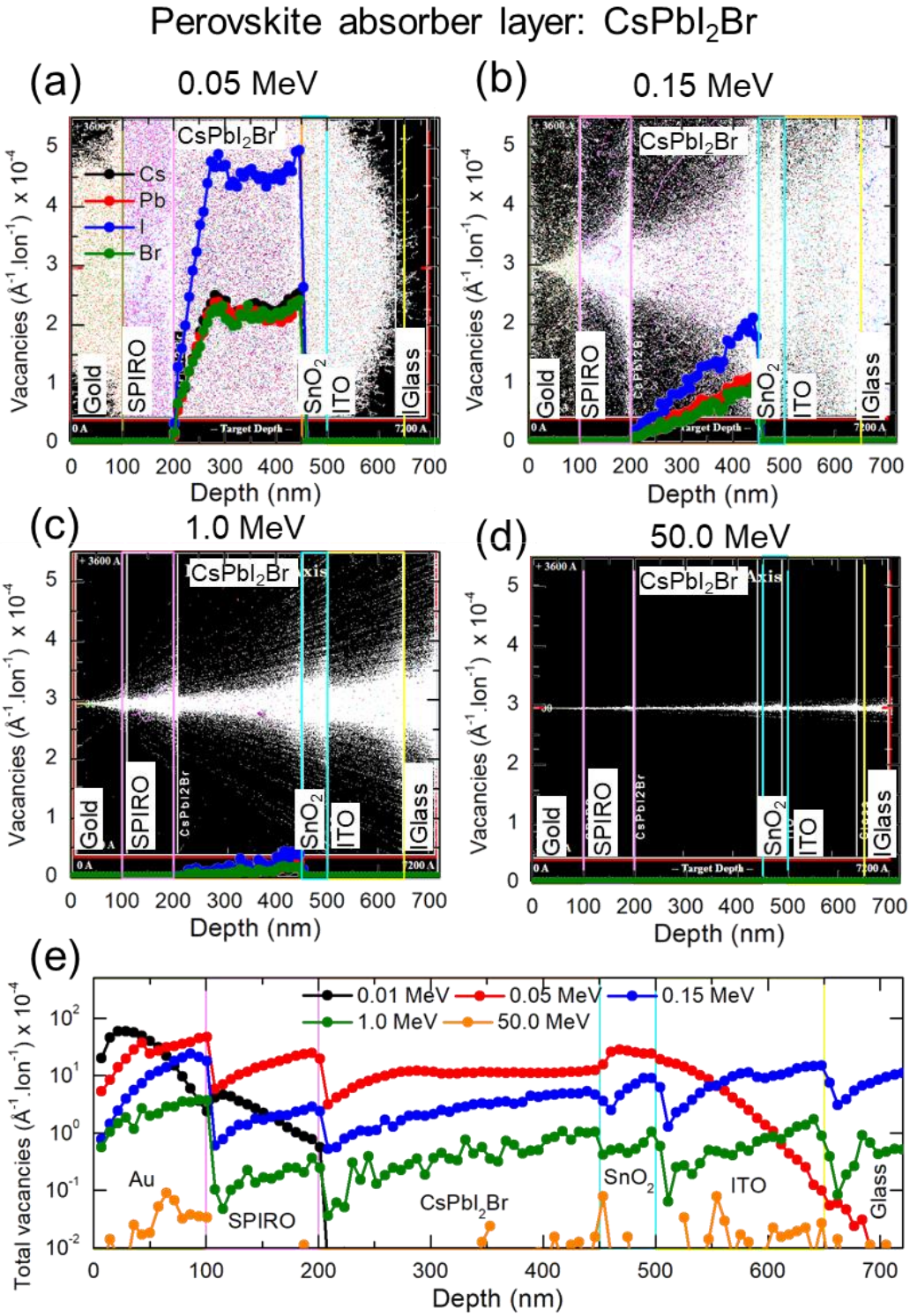

Figure S10. Simulated Proton Interaction with $CsPbI_2Br$ Perovskite Devices. a-d). Simulated proton straggling and the resulting vacancies formed due to dislocations of I, Br, Cl and Br atoms in $CsPbI_2Br$ solar cells. e). Vacancies formed in the full device stack. See Discussion below for details. Device architecture considered is: Au (100 nm)/SPIRO (100 nm)/$CsPbI_2Br$ (250 nm)/SnO_2 (50 nm)/ITO (150 nm)/glass (70 nm).

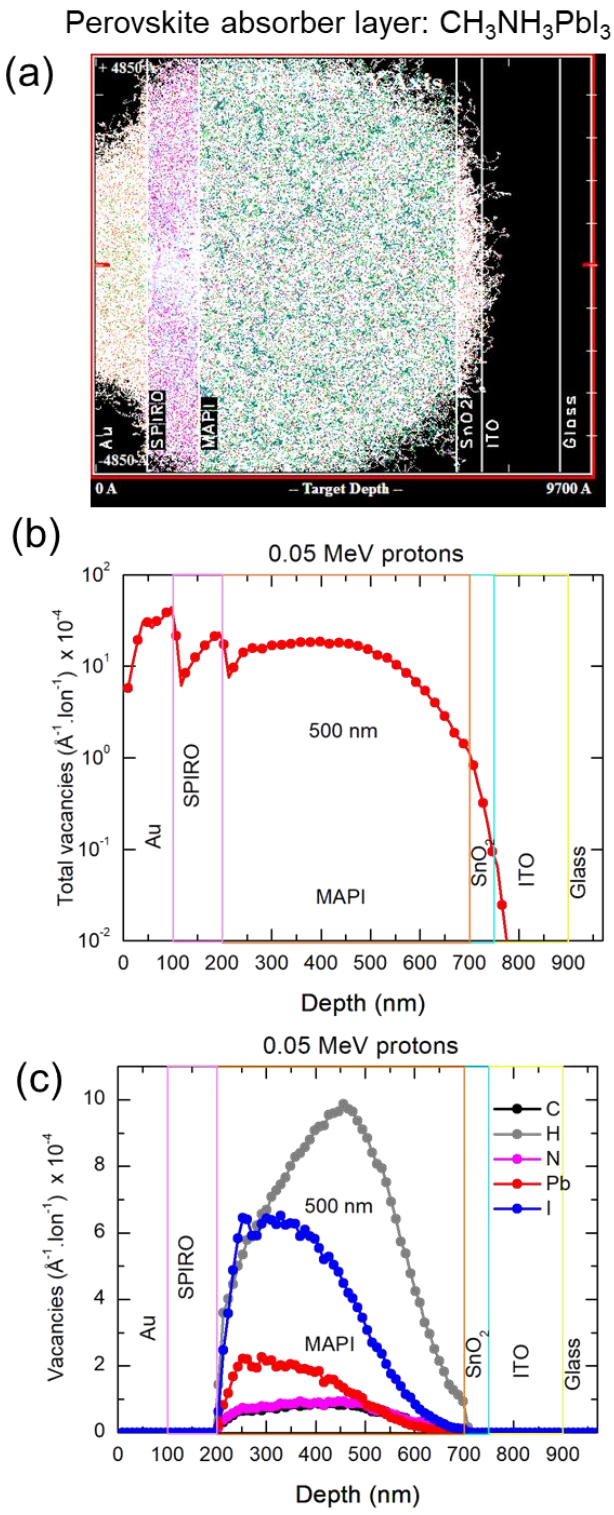

Figure S11. Simulated Proton Interaction with a $CH_3NH_3PbI_3$ Perovskite Device. (a) Proton straggling for $CH_3NH_3PbI_3$ solar cells, (b) vacancies created in the device, and (c) vacancies due to C, H, N, Pb, and I. Device structure considered is: Au (100 nm)/SPIRO (100 nm)/$CH_3NH_3PbI_3$ (500 nm)/SnO_2 (50 nm)/ITO (150 nm)/glass (70 nm).

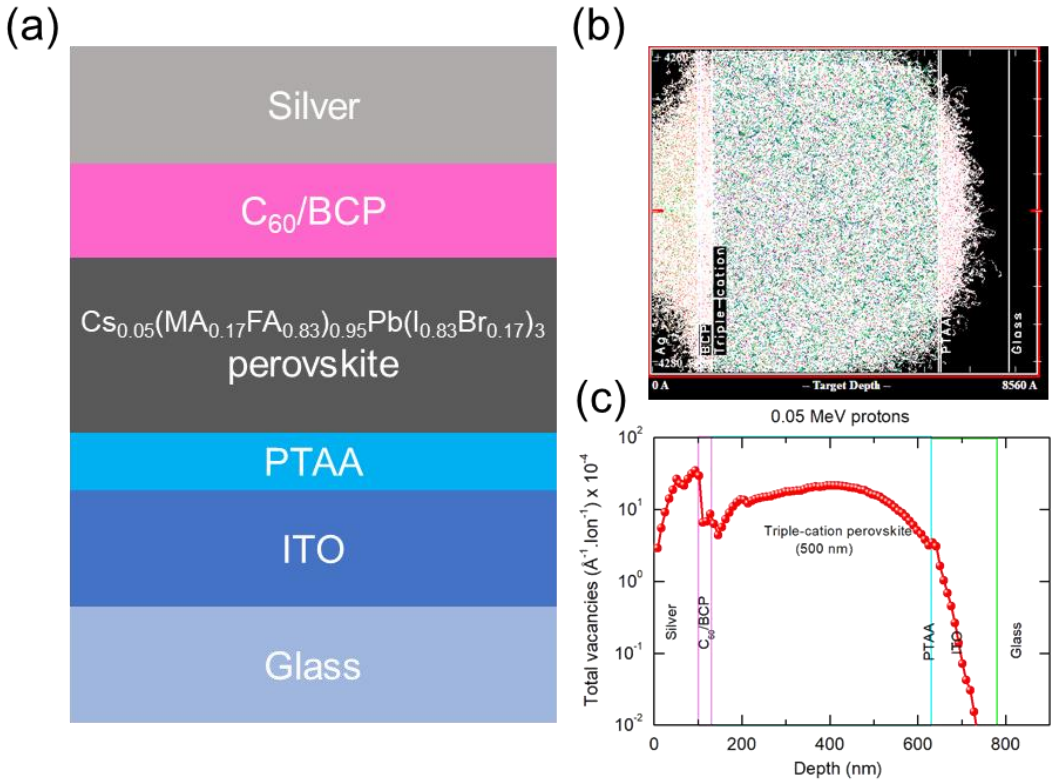

Figure S12. Simulated Proton Interaction with a *PIN* Perovskite Device. Proton interactions in a *pin* $Cs_{0.05}(MA_{0.17}FA_{0.83})_{0.95}Pb(I_{0.83}Br_{0.17})_3$ solar cell. (a) Device architecture considered for modeling. (b) SRIM/TRIM simulations showing straggling of 0.05 MeV protons incident from the silver electrode side. (c) Red line represents the total vacancies generated within the device stack and highlights that 0.05 MeV protons create a majority of vacancies inside the perovskite active layer, similar to the case of $CsPbI_2Br$ and *n-i-p* $Cs_{0.05}(MA_{0.17}FA_{0.83})_{0.95}Pb(I_{0.83}Br_{0.17})_3$ solar cells solar cells.

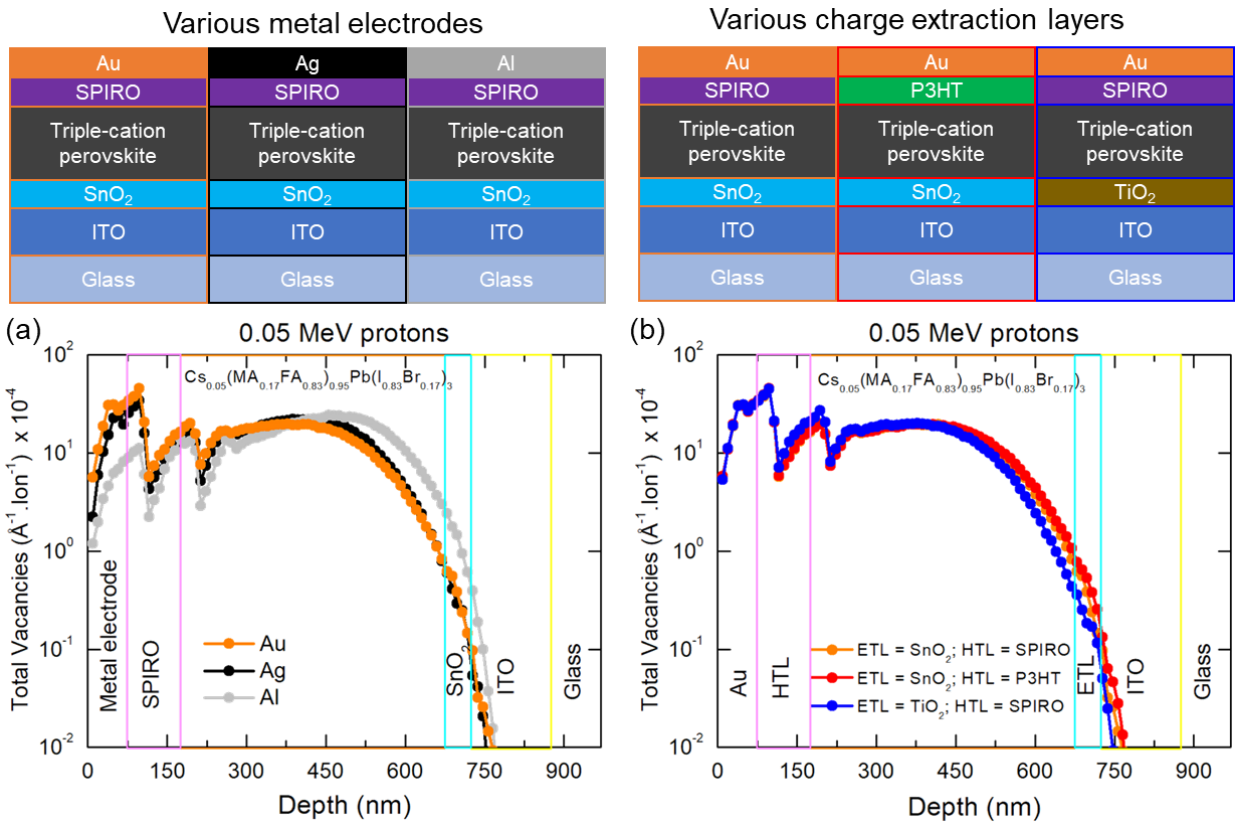

Figure S13. Vacancy Creation in Various Perovskite Device Architectures. SRIM simulations showing vacancy profiles within device stacks with (a) different metal electrodes, and (b) different charge extraction layers. Device stacks considered are shown in schematics above the figures.

Discussion:

Given the importance of metal electrode and charge extraction layers in the device stack, we also performed SRIM simulations on $Cs_{0.05}(MA_{0.17}FA_{0.83})_{0.95}Pb(I_{0.83}Br_{0.17})_3$ perovskite device stacks with various metal contacts (Ag and Al), a different hole-transporting layer (P3HT), and a different electron-transporting layer (TiO_2) to understand interaction of protons with these layers and defect formation. The vacancy profiles in these device stacks upon irradiation with 0.05 MeV protons are shown in Figure S13. Protons are found to create the smallest number of vacancies in the Al electrode compared to Au and Ag. Although Al has a significanty smaller atomic number (Z = 13) and its atoms have low binding strength compared to Au (Z = 79) and Ag (Z = 47), it has a vastly lower mass density of 2.7 g.cm^{-3} than Au (19.3 g.cm^{-3}) and Ag (10.49 g.cm^{-3}). A low mass density results in a smaller number of Al atoms per unit volume reducing the probability of interaction with protons. This implies that the incident protons do not lose sufficient energy while passing

through Al and can create more damage upon reaching the perovskite absorber. In fact, Figure S13a shows that for the perovskite solar cell with Al electrode has a larger number of vacancies inside the perovskite layer. This can potentially mean that Ag and Au electrodes can limit proton damage to the perovskite.

Similarly, given its higher mass density (1.4 $g.cm^{-3}$), SPIRO has higher vacancy profile compared to the lower mass density P3HT (1.1 $g.cm^{-3}$). As expected, perovskite active layer in the SPIRO device shows slightly less vacancies than the case of P3HT (Figure S13b). It is harder to compare electron transporters given that protons pass through them after traversing the perovskite, meaning their interaction with electron transporter layers does not affect the vacancy profile within the perovskite.

Table S1. Proton look-up table for ISS orbit.

Proton Energy (MeV)	**1-yr Fluence (cm^{-2})**	**5-yr Fluence (cm^{-2})**	**20-yr Fluence (cm^{-2})**	**1-yr DDD ($MeV.g^{-1}$)**				
				Triple-cation	MAPI	$CsPbI_2Br$	Si	InGaP
0.10	1.6E10	8.1E10	3.2E11	4.0E9	3.9E9	3.7E9	8.2E9	4.9E9
0.150	1.4E10	6.8E10	2.7E11	2.5E9	2.4E9	2.3E9	4.9E9	3.0E9
0.500	5.9E9	3.0E10	1.2E11	4.2E8	4.2E8	4.1E8	7.5E8	5.0E8
1.000	3.3E9	1.7E10	6.7E10	1.3E8	1.3E8	1.3E8	2.2E8	1.6E8
50.000	3.6E8	1.8E9	7.3E9	5.4E5	4.8E5	5.5E5	1.7E6	1.2E6
100.000	2.0E8	1.0E9	4.0E9	1.8E5	1.5E5	2.0E5	6.2E5	5.7E5

Discussion: Equivalent fluences can be calculated from the DDD values at two different proton energies. As an illustration, a fluence of 1.6E10 cm^{-2} for 0.10 MeV protons will result in a similar nuclear displacement damage in a $Cs_{0.05}(MA_{0.17}FA_{0.83})_{0.95}Pb(I_{0.83}Br_{0.17})_3$ solar cell as (4.0E9/1.8E5)*1.6E10 = 3.6E14 cm^{-2} fluence for 100 MeV protons. However, this 100 MeV proton fluence should not be used to simulate the effect of 0.10 MeV protons, since the electronic ionization (healing) scales differently. 100 MeV protons at a fluence of 3.6E14 cm^{-2} create significantly higher electronic ionization events than 1.6E10 cm^{-2} fluence of 0.10 MeV protons.

Indeed, the reverse is also true and lower energy protons should not be used for high-energy equivalence.

Annual fluences for various proton energies in equivalents of 0.1 MeV protons are calculated and shown in Table S2 for various PV technologies.

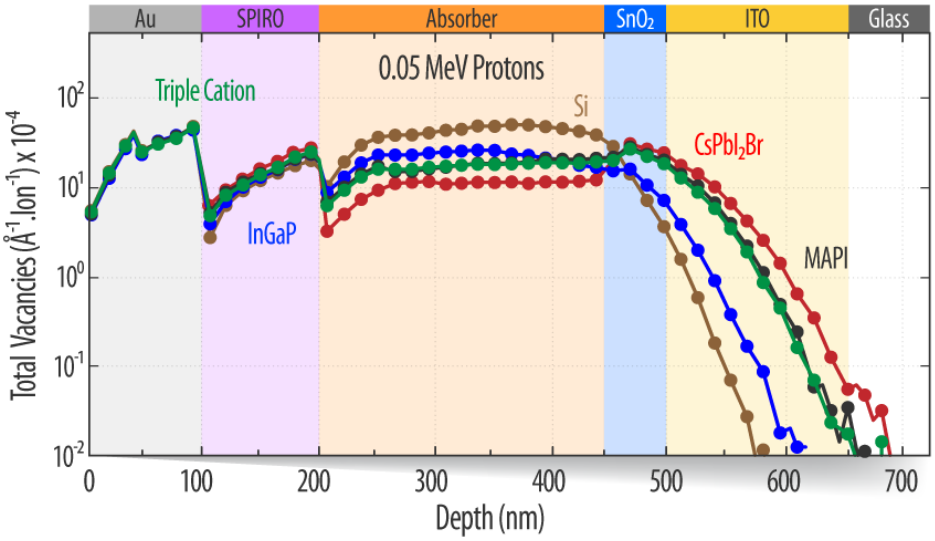

Figure S14. Defect Creation in Various Solar Cell Technologies. Comparison of vacancies formed in device stacks with perovskite absorbers ($Cs_{0.05}(MA_{0.17}FA_{0.83})_{0.95}Pb(I_{0.83}Br_{0.17})_3$, $CH_3NH_3PbI_3$, and $CsPbI_2Br$) and conventional PV absorbers (Si and InGaP), upon irradiation with 0.05 MeV protons and assuming constant thickness absorber.

Table S2. Equivalent annual fluences for ISS orbit for various PV technologies.

Proton Energy (MeV)	**1-yr Fluence (cm^{-2})**	**0.1 MeV Equivalent Annual Fluence (cm^{-2})**				
		Triple-cation	MAPI	$CsPbI_2Br$	Si	InGaP
0.10	1.6E10	1.6E+10	1.6E+10	1.6E+10	1.6E+10	1.6E+10
0.150	1.4E10	2.6E+10	2.6E+10	2.6E+10	2.7E+10	2.6E+10
0.500	5.9E9	1.5E+11	1.5E+11	1.4E+11	1.8E+11	1.6E+11
1.000	3.3E9	4.9E+11	4.8E+11	4.6E+11	6.0E+11	4.9E+11
50.000	3.6E8	1.2E+14	1.3E+14	1.1E+14	7.7E+13	6.5E+13
100.000	2.0E8	3.6E+14	4.2E+14	3.0E+14	2.1E+14	1.4E+14

Table S3. **Proton Energies Adjusted for Various Cover Glass Thicknesses.** Proton energies suggested for irradiation of perovskite solar cells after including a cover glass in the device stack. Proton energies in bold correspond to the reduced energies incident on the top metal electrode after the protons pass through the cover glass.

Cover glass thickness (μm)	**Proton energy (MeV) after 'cover glass correction'**				
	0.050	**0.075**	**0.100**	**0.150**	**0.200**
50	2.368	2.393	2.418	2.468	2.518
100	3.491	3.516	3.541	3.591	3.641
150	4.562	4.587	4.612	4.662	4.712
200	5.455	5.480	5.505	5.555	5.605
1000	13.457	13.482	13.507	13.557	13.607